Bulletin of the Seismological Society of America, Vol. 93, No. 5, pp. 2222–2235, October 2003

The Three-Dimensional Dynamics of a Nonplanar Thrust Fault

by David D. Oglesby and Ralph J. Archuleta

Abstract Advances in computational methodology have made it possible to explore the dynamics of earthquake rupture on nonplanar faults. Using a method that allows geometrical flexibility, we simulate in three dimensions the dynamics of a fault that has an abrupt change in dip with depth. Using a homogeneous prestress on both fault segments, we find that while the resultant final stress field is strongly influenced by the fault bend, the fault slip and low-frequency ground motion are relatively insensitive to the pure dynamic effects of the nonplanar fault. The ground velocity from the nonplanar fault is qualitatively quite similar to that of a planar fault with the same dip angle as the nonplanar fault's shallow segment. As the effects of multiple earthquakes accumulate on this fault, stress concentrations at the fault bend are compounded, but the effect of the free surface on the stress appears to approach a steady state. The results of this study imply that for the prediction of peak ground motion from faults that intersect the surface of the Earth, a bend in the fault at depth may not be a significant factor. The very long term effects of the fault bend are not fully determined, but could lead to complexity in the rupture and slip process in future events.

Introduction

In typical earthquake models, faults are often assumed to be straight, planar features. The reasons for this assumption are manifold, but the principal reason is simplicity: in order to avoid problems of mass continuity and the singular buildup of stress, it is convenient to assume that faults do not have bends or intersections with other faults. Furthermore, high-resolution information about fault structure at depth is often unavailable. Without compelling evidence of complicated structure, the most conservative assumption is often that of a planar fault. In addition, many common computational methods require orthogonal symmetry, so the numerical study of nonplanar faults is difficult. Kinematic forward models, using arrays of point sources, are able to take into account such features to within the resolution of the grid, but dynamic models with nonorthogonal fault geometry are much more difficult. However, structural geologists have long pointed to reflection seismology and other data as evidence that faults have bends and intersect other faults at nonorthogonal angles. In order to plan for possible earthquakes on such faults, it is necessary to determine if they behave differently from planar faults.

There are strong theoretical reasons to believe that nonplanar faults behave differently from planar faults. Faults with bends are an example of a shear structure for which the normal stress is not constant during rupture and slip. In a homogeneous whole space, slip on a fault does not modify the normal stress on the fault (Burridge, 1973). The constant normal stress of such a system is a result of the extreme symmetry of the geometry. The symmetry of a vertical fault in a laterally homogeneous medium also ensures that the normal stress on the fault does not change during rupture. However, the breakdown of this symmetry can cause the normal stress on the fault to vary with time, which in turn can have a great impact on fault behavior. One example of such symmetry breakage is the case of a fault with a nonvertical dip angle with respect to the free surface. Davis and Knopoff (1991), Mikumo and Miyatake (1993), Rudnicki and Wu (1995), Brune (1996), Nielsen (1998), Oglesby *et al.* (1998, 2000a,b), and Shi *et al.* (1998) have illustrated both the quasi-static and dynamic effects of nonvertical fault dip. These effects include greater fault motion for thrust/reverse faults than normal faults and greater motion on the hanging wall than on the footwall. Another example of a situation in which the normal stress can vary during an earthquake is the case of interacting parallel faults (Harris *et al.*, 1991; Harris and Day, 1993; Kase and Kuge, 1998; Harris and Day, 1999). In this case, the normal stress change induced on one fault by rupture on another can greatly affect the jumping of rupture across a fault step-over. The case of different material properties on either side of the fault can also lead to changes in normal stress (Andrews and Ben-Zion, 1997; Harris and Day, 1997; Ben-Zion and Andrews, 1998). Such a fault structure can support a stable pulselike rupture mode not present in a homogeneous medium.

A nonplanar fault with an abrupt change in dip or strike is another such system for which the normal stress is not constant in time during an earthquake. The reason for this effect is that the radiated stress field from one segment of the fault, when translated and rotated onto the other segment, will in general be resolved into both shear and normal components. Depending on the direction of the bend, rupture propagation direction, and fault slip, slip on one segment can either aid or hinder slip on the other segment. Andrews (1989) showed through static models that a bend in a 2D plane-strain fault causes a stress singularity proportional to 1 over the distance from the bend, as well as a kink (reduction) in the slip distribution near the bend. Both these effects are caused by the induced normal stress change due the nonplanar fault geometry. Bouchon and Streiff (1997) used a dynamic boundary integral method to examine a similar situation. They found that when the rupture crossed a bend from an orientation favorable to rupture to an orientation less favorable to rupture, the rupture front slowed down and produced less slip on the less favorable segment, leading to a noticeable effect in the final slip pattern. The bend also produced noticeable radiation phases, as well as a decreased rise time. Kase and Kuge (1998) and Magistrale and Day (1999) have both modeled the dynamics of faults with orthogonal segmentation and found that the ability of the rupture to propagate across the segment boundaries was a complicated result of the initial stress fields, as well as directivity and other dynamic factors.

Aochi *et al.* (2000) used a boundary integral equation method to model the dynamics of nonplanar faults in three dimensions with more generalized nonorthogonal fault segment orientation. They found that the most important factor in determining the dynamics of the fault was the difference in static shear stress on differently oriented fault segments, assuming that the shear stress was resolved on the fault segments from a constant tectonic stress field in the medium. However, they did not model the effects of dynamic changes in normal stress due to the bend. Aochi and Fukuyama (2002) used a similar method to model the dynamics of the 1992 *M* 7.3 Landers, California, earthquake and found that the nonplanar fault structure (with a tectonic stress field that changed orientation with the overall change of fault strike) could account for the large-scale features of the inferred slip distribution, as well as match qualitatively some nearby low-frequency strong motion records. Aochi *et al.* (2002) performed a 3D dynamic analysis of a branching fault and concluded that the omission of dynamically changing normal stress in the previous two studies was valid, because in their models the ability of rupture to propagate to the different branches was dominated by the change in shear, rather than normal stress. However, they did not investigate the issue of the effect of normal stress on the final slip distribution. Harris *et al.* (2002) also modeled the rupture of a nonplanar fault (during the 1999 Izmit, Turkey, earthquake) and found that a 22.5° change in fault strike at the eastern end of the fault did not serve as a barrier to rupture. Poliakov *et al.* (2002) and Li *et al.* (2003) have further investigated the dynamics of branched fault systems, showing that the combined effects of static and dynamic shear and normal stresses interact with the fault geometry to determine which path a rupture will take.

An additional issue that is of great importance for a nonplanar fault is the effect of multiple earthquake cycles. As slip accumulates near the fault bend, a space problem will result, and stresses will start to build up. Andrews (1989) showed with his static models that fault bends should be unstable over multiple earthquake cycles and could lead to the formation of secondary faults to relieve the built-up stress at the corners. Using a 2D static model, Nielsen and Knopoff (1998) simulated the long-term evolution of a fault system with changes in strike. They included a form of aseismic relaxation to keep stresses from approaching infinity at the fault bends. Their results showed that the changes in strike greatly affected the long-term behavior of the system and acted as both nucleation zones and barriers to rupture. However, this study did not include full inertial dynamics. Lapusta *et al.* (2000) included inertial dynamic effects as well as a full model of the interseismic and nucleation periods in their study of the long-term evolution of a 2D planar strike-slip fault. They found that the fault produced a spectrum of earthquake sizes but eventually settled into a somewhat repeating pattern. The present work takes a middle ground between these two studies: we simulate the dynamics of multiple events, but we utilize only a rudimentary model of the interseismic period and nucleation. Our goal is to study how the effects of nontrivial fault geometry may accumulate over multiple earthquake cycles and point toward future work in modeling the long-term dynamics of faults with nontrivial geometry.

Simulation Method

We use the 3D finite-element method (Whirley and Engelmann, 1993; Oglesby, 1999) to simulate the dynamics of a nonplanar fault. This method has the advantage of complete freedom of fault geometry, as well as the ability to model full 3D variations in fault properties and rheological structure. The geometry of the fault is shown in Figure 1. We choose a fault configuration similar to that of Heaton and Helmberger (1979) in their model for the 1971 *M* 6.6 San Fernando, California, earthquake. However, we are not attempting to produce a model for the specific San Fernando event. Rather, we are attempting to explore the effect of this particular fault geometry on the dynamics of the earthquake process and ground motion. Accordingly, we use a very simple model for both the material and the fault prestresses: we use a homogeneous half-space and an (initially) homogeneous prestress distribution on the fault in order to isolate the purely geometrical effects on the fault dynamics.

The material and computational parameters in our models are given in Table 1. Our fault friction law is given by

$$\begin{aligned}\tau(\vec{r},t) &\leq \mu_s \sigma_n(\vec{r},t) \text{ (for static friction)} \\ \tau(\vec{r},t) &= \mu_d(\vec{r},t)\sigma_n(\vec{r},t) \text{ (for sliding friction),}\end{aligned} \quad (1)$$

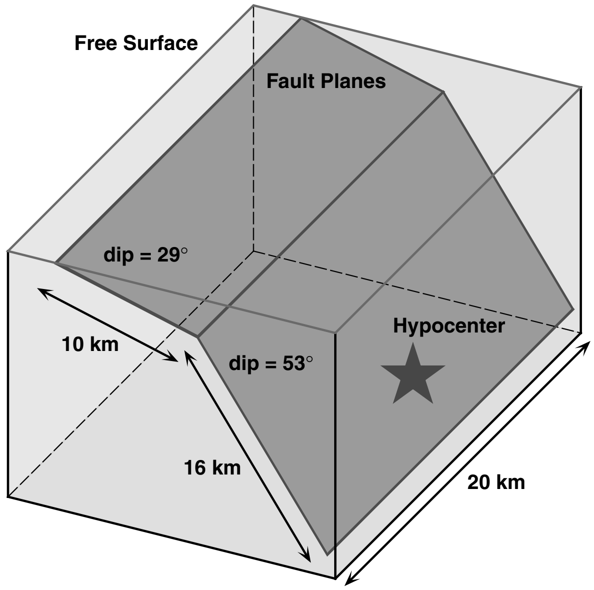

Figure 1. Nonplanar fault geometry used in the current work. The fault is composed of two segments, with the upper segment having a shallower dip. Nucleation is on the lower segment.

Table 1
Material and Computational Parameters

Fault width (down dip)	26,000 m
Fault length (along strike)	20,000 m
Fault dip (shallow/deep)	29°/53°
Shear prestress	1.6×10^7 Pa
Normal prestress	3.0×10^7 Pa
Static frictional coefficient	0.7
Sliding frictional coefficient	0.3
Density	2800 kg/m^3
Shear modulus	3.65×10^{10} Pa
Poisson's ratio	0.2576
V_p	6300 m/sec
V_s	3600 m/sec
Element width on fault	500 m * 500 m
Maximum frequency	~0.6 Hz
Critical slip distance	0.4 m

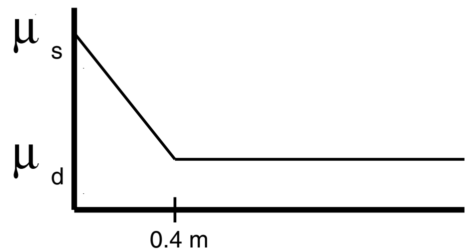

Figure 2. Slip-weakening friction law used in the current study. The frictional coefficient drops linearly from its static value to its sliding value as it slips a critical distance.

where τ is the frictional shear stress on the fault, μ_s and μ_d are the static and sliding frictional coefficients, and σ_n is the effective (lithostatic minus pore fluid pressure) normal stress across the fault. Note that all these variables (with the exception of the static frictional coefficient) are functions of position and time, with the sliding frictional coefficient being an explicit function of slip (and thus an implicit function of time). Before rupture at a point, when the static frictional condition holds, the stress can assume any value up to the static shear strength. At rupture time, when the stress required to keep the fault slip free is exceeded, the shear stress is assigned via the second part of equation (1). The sliding frictional coefficient decreases from its initial to its final level (i.e., between static and sliding friction) via a simple linear slip-weakening law (Ida, 1972; Andrews, 1976) with a critical slip distance of 40 cm (thus allowing the stress drop to take place over at least three elements), as shown in Figure 2. Experiments with different slip-weakening distances do not significantly affect the results. We allow slip to take place in any direction in the fault plane; the frictional stress is always applied in the direction opposite that of the instantaneous slip velocity. The fault is healed when the frictional stress is enough to cause the slip velocity to pass through zero in the next timestep (similar to Andrews [1999]).

Some remarks are in order concerning our choice of stress field. Using the same shear and normal stresses on both fault segments is not the same as using a constant tectonic stress field, as is assumed in most previous studies of nonplanar faults (e.g., Bouchon and Streiff, 1997; Aochi *et al.*, 2000; Harris *et al.*, 2002). The current model is more similar to that of Kase and Kuge (1998), who had the same shear and normal stresses on both of their nonplanar fault segments. However, due to their orthogonal fault geometry, their model is consistent with a constant tectonic stress field. Our approach is also somewhat similar to that of Aochi and Fukuyama (2002), who had a tectonic stress field that changes orientation in roughly the same way as the strike of the 1992 Landers earthquake. In our case, we separate out the effect of changes in the static stress field (due to fault orientation or any other factors) from the effect of changes in the dynamic stress field due to fault rupture and slip. The former effect has been studied in detail (starting with Day [1982]), and we do not wish to confuse the two effects in rupture behavior in our models. However, the case of nearly constant shear and normal stresses (or at least constant relative shear and normal stress orientations) on nonplanar fault segments is not artificial. Zoback *et al.* (1987) have argued that the stress field near the San Andreas fault changes orientation along its length so that the maximum compressive stress is almost always nearly perpendicular to fault strike. This observation is equivalent to saying that the San Andreas fault is quite weak, and it is the best physical interpretation for our model as well. Fault behavior such as this has also been shown in the work of Mount and Suppe (1992) and

Axen (1992). The presence of weak faults in southern California was further argued by Hardebeck and Hauksson (2001). Finally, we assert that the stress field on a fault is due to a combination of tectonic stresses, lithostatic stresses, and the entire earthquake history on the fault, rather than simply tectonic stresses alone. Thus, our stress model, while different from that used in many previous models, is probably no less reasonable an approximation than the assumption of constant tectonic stress. However, when drawing conclusions about ground motion from our models, we will address the issue of model generality again. Henceforth, the case in which we use the same shear and normal stresses on both fault segments will be denoted the "nonrotated" case. The case in which the shear and normal stresses are drawn from a constant tectonic stress field and resolved onto the individual fault segments will be denoted the "rotated" case.

Prior to our exploration of the effects of nonplanarity, we also perform a check to verify that our assumption of constant (rather than rotated) shear and normal stresses on both segments does not greatly bias our results. Due to its very steep dip angle, a uniform tectonic stress field that is favorable for the upper fault segment to rupture also is highly unfavorable for the lower fault segment to rupture. This effect has been noted by Sibson and Xie (1998), who showed that thrust faults with dip angles greater than 50° are essentially at the point of frictional lockup and require fluid overpressurization to allow slip. To test the effect of rotating the stress field versus having constant shear and normal stress on both segments, we compare our constant stress model to two models where the shear and normal stresses are rotated to the orientation of the lower segment and then additional pore fluid pressure is added to reduce the effective normal stress in the calculation, thus allowing the lower segment to slip in the manner suggested by Sibson and Xie (1998). A summary of the stresses used in these simulations is given in Table 2. At the depth of the fault bend, lithostatic normal stresses should be on the order of 1×10^8 Pa, so in assuming a normal stress of roughly 3×10^7 Pa, we are already (on the upper fault segment) assuming a pore fluid pressure on the order of 7×10^7 Pa. Thus, adding an additional 0.9×10^7 to 1.1×10^7 Pa of pore fluid pressure is actually quite a small additional increment and consistent with our assumption that the stress drop not vary drastically with depth. This additional pore fluid pressure appears to be required by our geometry, but may not be required by all conceivable fault geometries.

In our models, we explicitly account for dynamic changes in normal stress due to the nonplanar fault via equation (1). We also allow slip in all fault-parallel directions. As in the case of Bouchon and Streiff (1997), the finite discretization size of the model means that the fault bend is not a perfectly sharp corner: the change in dip is effectively smoothed out over roughly one element size, or 500 m. Rupture nucleation is achieved by temporarily increasing the shear stress over a small (3.4-km radius) region of the fault to the level of the yield stress.

Table 2
Stresses Used in Comparison between Rotated and Nonrotated Stress Models

Horizontal principal stress	5.9×10^7 Pa
Vertical principal stress	2.1×10^7 Pa
Shear prestress (upper segment)	1.6×10^7 Pa
Normal prestress (upper segment)	3.0×10^7 Pa
Shear prestress (lower segment; rotated)	1.8×10^7 Pa
Normal prestress (lower segment; rotated)	4.5×10^7 Pa
Maximum additional fluid pressure	1.1×10^7 Pa
Minimum additional fluid pressure	9.0×10^6 Pa
Normal prestress (lower segment; maximum additional fluid pressure)	3.4×10^7 Pa
Normal prestress (lower segment; minimum additional fluid pressure)	3.6×10^7 Pa

To further isolate the effects of a fault bend, we simulate the dynamics of two planar faults with dip angles equal to the dip angles of the two segments of the nonplanar fault (29° and 53°, respectively, for the upper and lower fault segments). For all faults we use the same normal and shear stress magnitudes (Table 1). All faults have the same length and width. The only differences are the dip angles and the presence of a bend.

To investigate the effect of multiple earthquakes on the fault system, we used a very rudimentary ("zero-order") means of accounting for the gradual buildup of stress in the interseismic period. We started with the final stress left after the first simulated earthquake. The first step was to remove the effect of numerical noise by passing the fault stresses through a boxcar averaging process, by which the stress at a point was set equal to the average of its four neighbors. Physically, this process could serve as an extremely rudimentary form of aseismic stress relaxation. Then, to simulate the result of loading in the interseismic period, the shear stress was multiplied by a constant factor (across the entire fault plane) such that the relative fault strength in the nucleation region, $S = \sigma_y - \sigma_0/\sigma_0 - \sigma_f$ (where σ_y is yield stress, σ_0 is initial shear stress, and σ_f is the sliding frictional stress), is equal to 0.71, its value for the initial event. Thus, we approximate the stress buildup as being a constant increase over the whole fault. Finally, fault rupture was nucleated in exactly the same manner as the initial event. Thus, one can think of our multicycle models as taking place on a fault where the initial stress is related simply (via a multiplicative constant) to the final stress from the previous event. The only exception to this overall process is the third event, for which rupture was initiated at two points near the surface rather than at depth. As will be explained in the results, these areas were brought past the stress failure criterion in the shear stress scaling process, although shallow nucleation of a thrust earthquake is unlikely in nature (Scholz, 1990). This stress buildup method is rather *ad hoc* and should be considered a first step toward a combined static/dynamic earthquake simulation method, which would accurately calculate the loading and nucleation processes.

Comparison of Ground Motion for Rotated versus Nonrotated Stress Field

To show that our subsequent simulations with constant (nonrotated) shear and normal stresses on the top and bottom segments do not substantially bias our results, we first present the results of our comparison between a rupture model with nonrotated stresses and one in which the stresses have been rotated and an additional amount of pore fluid pressure has been added to allow rupture propagation. The peak ground velocity resulting from three such models are compared in Figure 3. In this figure and in all ground-motion velocity figures to follow, ground motions are low-pass filtered to 0.6 Hz, the approximate maximum frequency in these simulations, assuming 10 grids per wavelength. The top panel shows the ground motion for the nonrotated (constant shear and normal stress) model. The middle panel shows the results for the rotated case in which the maximum amount of pore fluid pressure (1.1×10^7 Pa) is added to the normal stress, and the bottom panel shows the results for the rotated case in which the minimum amount of pore fluid pressure (9.1×10^6 Pa) is added. It should be noted that in the middle panel, S is the same as for the upper segment (0.71), whereas in the lower panel, S is increased to 0.98. Thus, in the bottom case the lower segment is less favored for rupture. Inspection of this figure clearly shows that there is very little difference in the peak ground motion between these three models. A comparison of the ground motion at the point marked by a triangle in Figure 3 is shown in Figure 4. There are small differences between the synthetic seismograms for the three cases, but the most prominent differ-

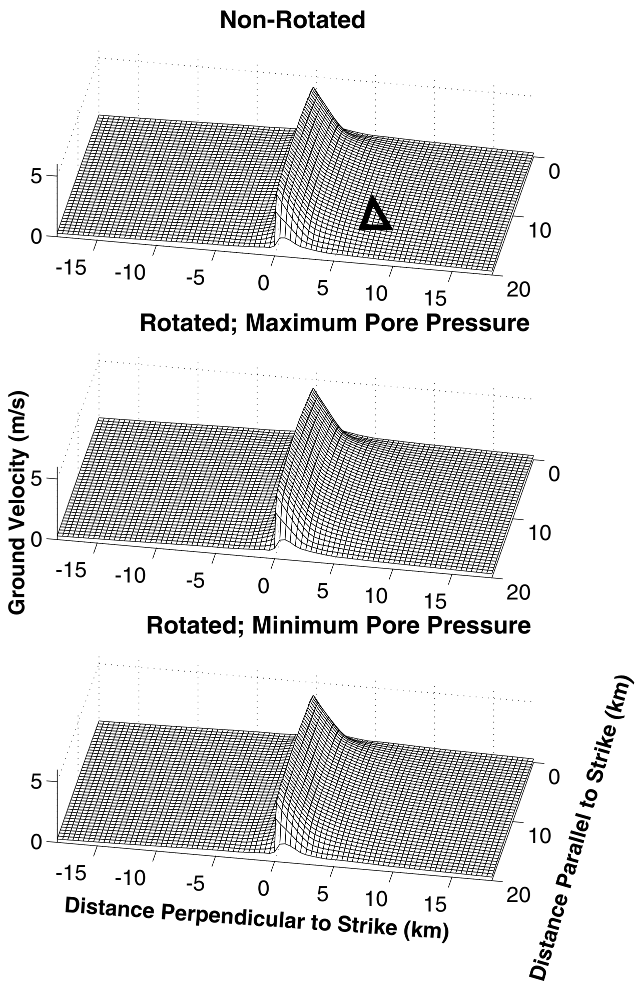

Figure 3. Peak ground velocity amplitude for the nonplanar fault in the cases of nonrotated shear and normal stress (top panel), rotated stress with the maximum amount of additional pore pressure (middle panel), and rotated stress with the minimum amount of additional pore pressure (bottom panel). Faults intersect the surface at 0 km perpendicular to strike and dip to the right (hanging walls have positive strike-perpendicular coordinates). The ground-motion patterns are quite similar in all cases. The location at which synthetic seismograms are later calculated are marked with a triangle on the top panel.

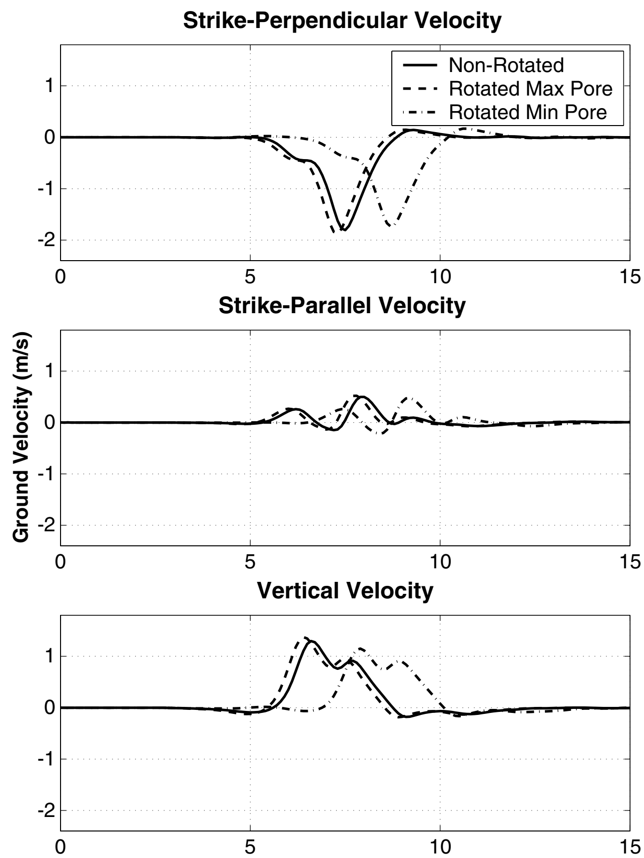

Figure 4. Synthetic ground velocity records for a point on the hanging wall approximately 15 km along strike and 3 km away from the fault trace (triangle on Fig. 3). This figure shows a comparison between nonrotated stresses, rotated stresses with maximum amount of additional pore pressure, and rotated stresses with minimum amount of additional pore pressure. All synthetics are quite similar, with the exception of a time shift for the rotated cases, which are less favorable to rupture.

ence is that the rotated models produce ground motion that is shifted later in time, due to the lower fault segment being less favored for rupture. The observation that the stress on the lower segment makes little difference in the ground motion at low frequencies serves to validate our subsequent models, in which we assume for simplicity that the upper and lower segments have the same shear and normal stresses. However, we will discuss again the possible effects of our assumed stresses at the end of this article.

Results for Initial Event using Homogeneous Stress

The effect of the change in dip (bend) on the fault can be seen in Figure 5, which shows two snapshots of slip rate (the amplitude of the 2D slip rate vector). In the top panel, the rupture front is crossing the bend at 10 km down dip. The slip rate at the bend is not as large as on other parts of the fault, but there is little other evidence of the presence of a geometrical discontinuity. There is no obvious healing pulse or other signal being radiated from the fault bend. In this model, rupture proceeds across the fault bend without difficulty. In the bottom panel, we see the amplification of slip rate due to the effect of the free surface (Brune, 1996; Oglesby *et al.*, 1998, 2000a,b; Shi *et al.*, 1998).

The effect of the fault bend on the system can be seen more clearly in the final slip pattern for this event. Figure 6 compares the final slip distributions for the nonplanar fault, the 29°-dipping fault, and the 53°-dipping fault. The nonplanar fault displays a clear kink in its slip distribution at the bend, although the slip at the bend is nonzero. This slip pattern is quite similar to that seen in the static results of Andrews (1989). In contrast, the two planar faults display slip that grows monotonically as the fault approaches the free surface, exactly as in Oglesby *et al.* (2000b). It is not clear if a slip inversion, with its limited resolution, would be able to distinguish between these three cases. This observation brings up the first hint that the effect of the bend may

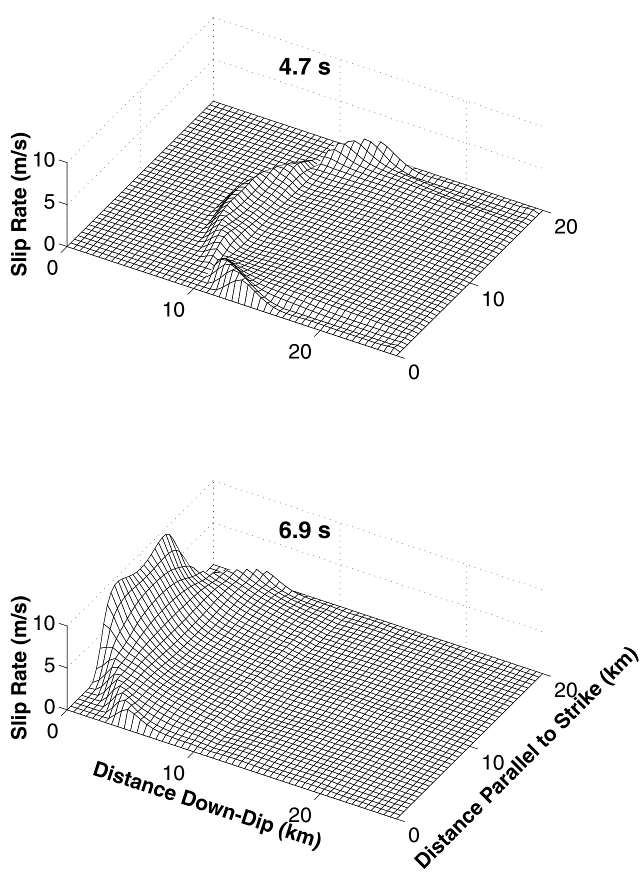

Figure 5. Snapshots of slip velocity on the nonplanar fault. The free surface is at 0 km down dip, and the change in dip (bend) is at 10 km down dip. At 4.7 sec, the rupture front is crossing the fault bend. The fault bend experiences a lower slip rate than surrounding points, but the rupture has no difficulty passing through the bend. At 6.9 sec, the rupture front experiences great amplification when it reaches the free surface.

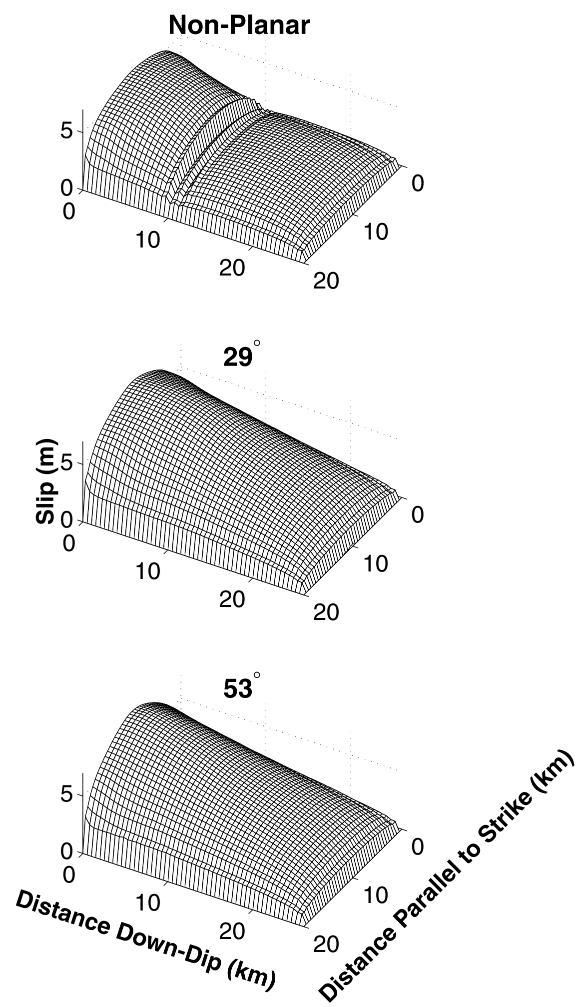

Figure 6. Final slip distributions for the nonplanar, 29°-dipping, and 53°-dipping faults. The effect of the bend can be seen as a kink in the slip distribution of the nonplanar fault. All three slip distributions are otherwise qualitatively similar.

be smaller than the effect of the free surface on this simulated earthquake.

Of particular importance for the purposes of seismic hazard prediction is the effect of fault geometry on the ground motion from this earthquake. Figure 7 compares the peak ground velocity (maximum amplitude of the 3D ground velocity vector) for the cases of the nonplanar, 29°-dipping, and 53°-dipping faults. All three faults display the basic pattern shown in Brune (1996), Oglesby *et al.* (1998, 2000a,b) and Shi *et al.* (1998): the ground motion is strongly peaked at the fault trace, with much greater motion on the hanging wall than on the footwall. It is also quite clear that the peak velocity pattern for the nonplanar fault much more closely resembles the pattern of the 29°-dipping fault than the 53°-dipping fault. This observation strongly implies that the angle that the nonplanar fault makes with the surface is the dominant factor in determining the peak ground motion. The effect of the more deeply buried steeper fault segment is considerably less important, at least very close to the fault trace.

Even though there are great similarities in peak ground motion between the nonplanar and 29°-dipping faults, it is still possible that the detailed ground motion is quite different for these two geometries. Thus, it is useful to examine some sample synthetic ground motions from these faults. Figure 8 shows the particle velocity at a point on the hanging wall approximately 15 km along strike and 3 km away from the fault trace. The synthetics are rather similar, with the exception of the strike-perpendicular (horizontal) compo-

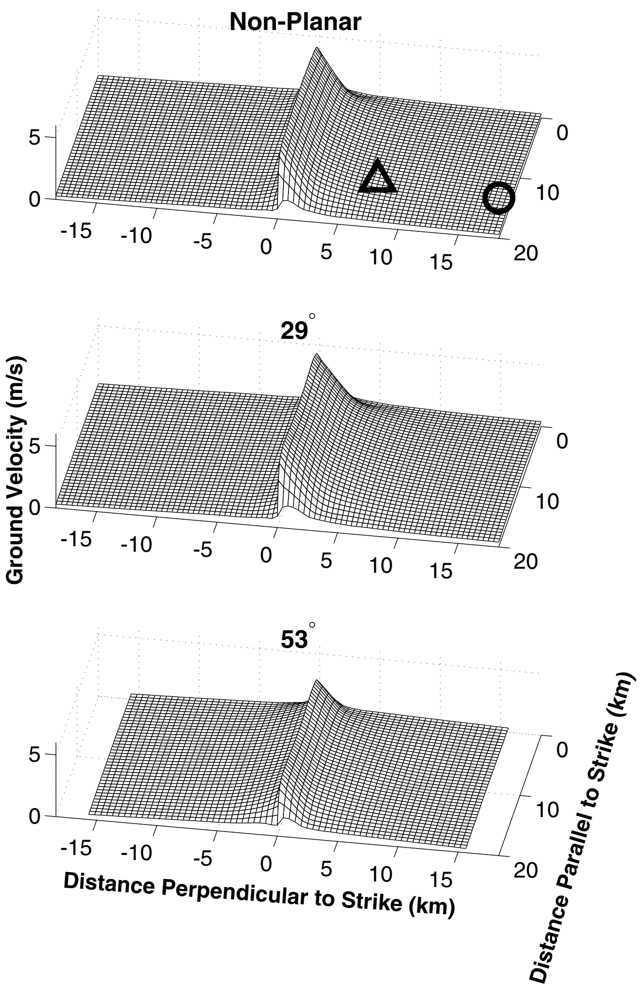

Figure 7. Peak ground velocity amplitude for the nonplanar, 29°-dipping, and 53°-dipping faults. Faults intersect the surface at 0 km perpendicular to strike and dip to the right (hanging walls have positive strike-perpendicular coordinates). The ground-motion pattern is quite similar for the nonplanar and 29°-dipping faults and different for the 53°-dipping fault. All three ground motions display typical features associated with the dipping fault geometry. The locations at which synthetic seismograms are later calculated are marked with a triangle and circle on the top plot.

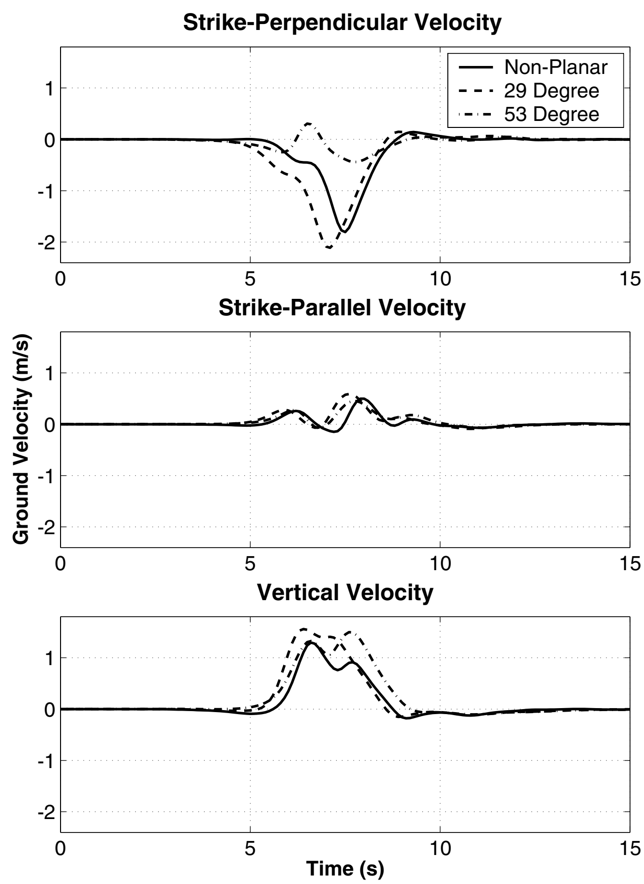

Figure 8. Synthetic ground velocity records for a point on the hanging wall approximately 15 km along strike and 3 km away from the fault trace (triangle on Fig. 7). This figure shows a comparison between the nonplanar fault, 29°-dipping fault, and 53°-dipping fault. While the records are similar in the strike-parallel and vertical components, the strike-perpendicular components show a great similarity between the nonplanar and 29°-dipping fault. The 53°-dipping fault produces qualitatively different ground motion.

nents of motion. For this component, the ground motion from the nonplanar fault is quite similar to that of the 29°-dipping fault, with the motion of the 53°-dipping fault quite dissimilar. Unlike in the case of Bouchon and Streiff (1997), there is no obvious signal or pulse from the rupture front hitting the fault bend. One obvious reason is that there is no change in the static stress at the bend, unlike in the previous study. Another important reason is the 3D nature of the current model: because of the arc shape of the rupture front, the collision of the rupture front with the bend takes place over many seconds, smearing out any possible signal. The similarity between the synthetics from the nonplanar and 29°-dipping faults is perhaps not very surprising, because the ground motion at a point is likely to be dominated by the part of the fault closest to it, especially for a shallow-dipping fault. Perhaps more surprising is the similarity of the synthetics in Figure 9 for a point farther away from the fault trace. This point is on the hanging wall, approximately 15 km along strike and 13 km away from the fault trace. Although smaller in amplitude, these synthetics show a pattern very similar to that of the closer-in synthetics: there is great similarity between the ground motion from the nonplanar fault and the 29°-dipping fault, and both are more dissimilar to ground motion from the the 53°-dipping fault. This is true even though the point in question is farther away from the fault trace than the bend in the nonplanar fault. Differences between the nonplanar fault motion and the 29°-dipping fault motion are mostly matters of different delay times rather than amplitude or phasing. Taken together, these results show that at least for low frequencies, the near-source ground motion from a thrust fault is dominated by the effect of the fault's angle with the free surface.

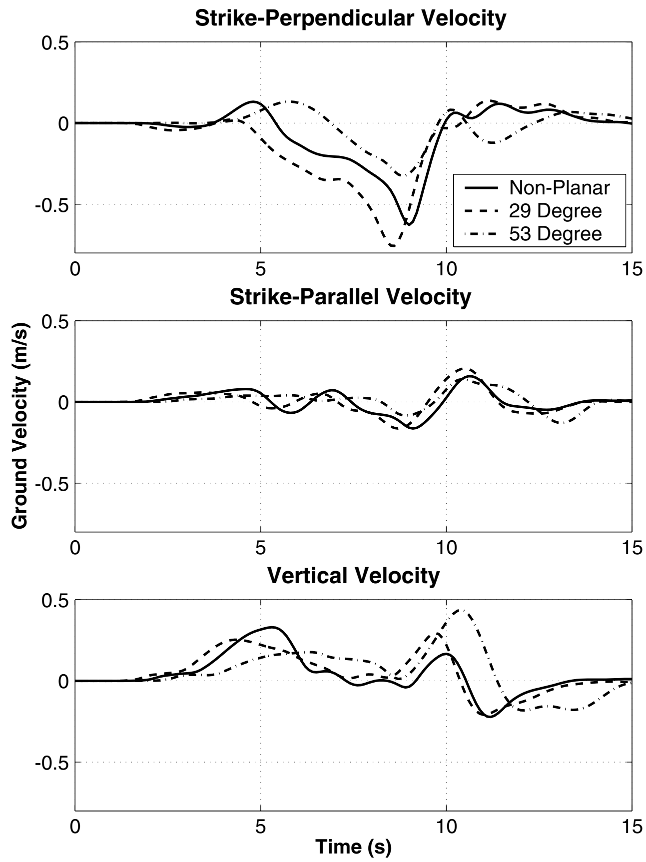

Figure 9. Synthetic ground velocity records for a point on the hanging wall approximately 15 km along strike and 13 km away from the fault trace (circle on Fig. 7). This figure shows a comparison between the nonplanar fault, 29°-dipping fault, and 53°-dipping fault. Even when sampled relatively far from the fault, the ground motion is more similar between the nonplanar and 29°-dipping faults than with the 53°-dipping fault.

Results for Multiple Events

The preceding results imply that the bend in the fault is of secondary importance compared to the effect of the free surface on fault slip and ground motion. However, the previous models assumed completely homogeneous stresses, which are unlikely to occur in nature. The initial stress field that an earthquake sees is the result of every past earthquake on that fault system, as well as whatever physical processes take place in the interseismic period. To investigate the effects of multiple earthquakes on the development of stress, slip, and ground motion, we have simulated three earthquake events on the nonplanar fault. The evolution of the stress field for this system is shown in Figure 10. The top row shows the initial stress field prior to the first event. After the first event, the thrust and normal stress are greatly reduced in the near-surface segment, in agreement with the results of Oglesby *et al.* (2000a,b). There is further decreased thrust stress near the fault's upper corners and a small amount of induced strike-slip stress near the fault bend and at the fault's upper corners. The most obvious feature is the effect on the normal stress at the fault bend. In agreement with the sense of slip on the fault, the normal stress is greatly increased just below the bend and greatly decreased just above the bend. This pattern is in accordance with the results of Andrews (1989). Because the sliding frictional shear stress is proportional to the normal stress, this pattern is also manifested in the thrust stress. As seen in the third row, the second event serves to amplify this stress buildup. It should be pointed out that even with the strongly inhomogeneous stress near the bend, the second earthquake has no difficulty rupturing around the bend toward the surface. The normal stress near the free surface is also further decreased, showing that the effect of the free surface on the stress also builds up in the second event. Another interesting feature with repercussions for the third event is the high stress in the upper corners of the fault. The reason for the stress buildup here is that these areas, due to their decreased shear stress after the first event, did not rupture in the second event. Thus, their shear stress is increased by slip on the rest of the fault. Because of the increased stress on these points, the stress-scaling process that leads to a third earthquake causes these areas to exceed

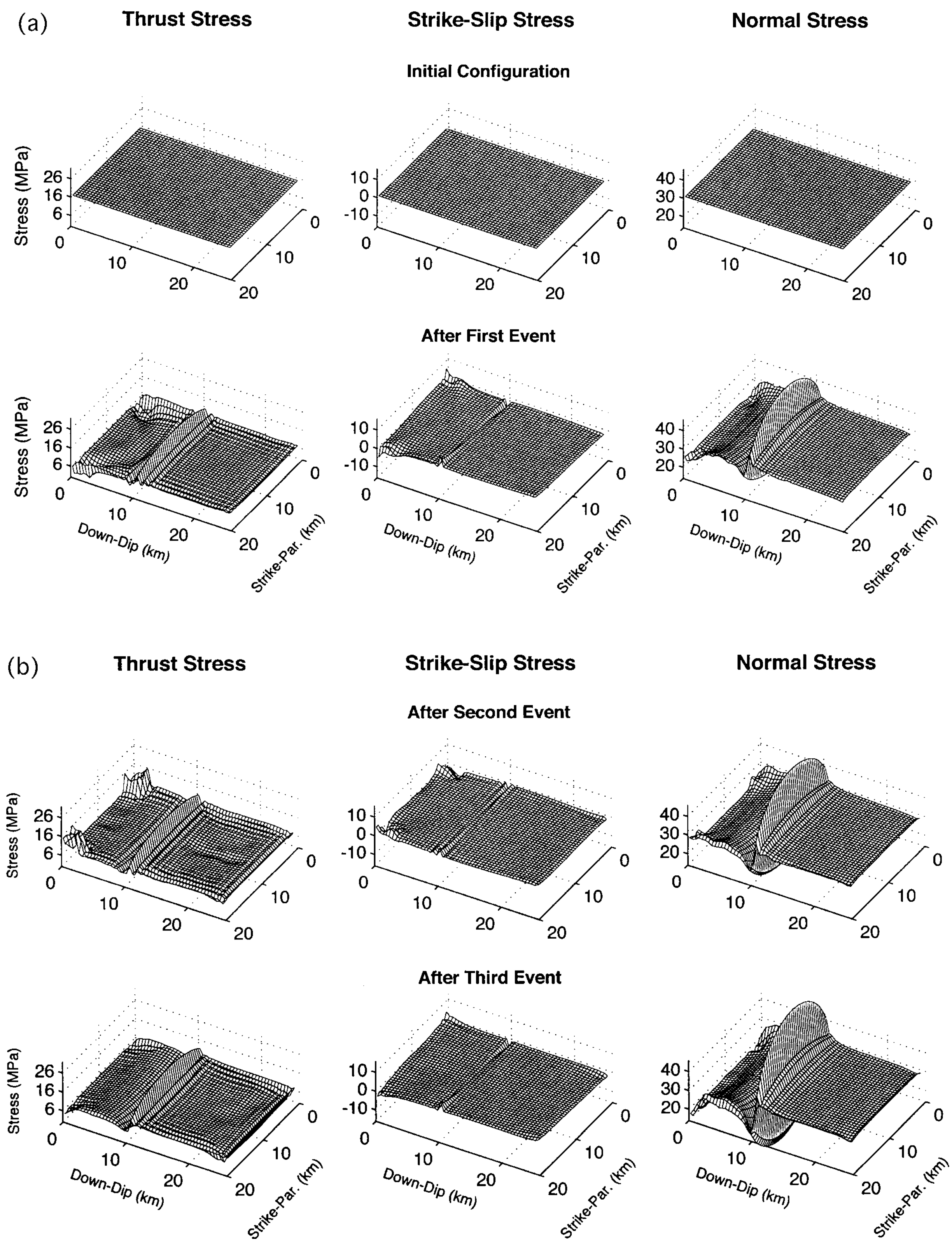

Figure 10. The evolution of stress on the nonplanar fault over three earthquakes. As the events occur, the stress buildup at the fault bend increases, while it appears that the stress at the free surface may approach a steady state. (a) Before and after the first event. (b) After the second and third events.

the yield stress and nucleate rupture near the surface. This shallow nucleation is quite unlikely to occur in nature (Scholz, 1990), but is included in the results for self-consistency. The presence of shallow nucleation is perhaps indicative of the effect of our simplifying assumptions in the current models, such as depth-independent fault stress and strength, as well as our constant scaling of the shear stress in the interseismic period. Regardless, even with nucleation taking place in a different location from the other two events, this event still ruptures through the bend to cause the whole fault to slip. After this third event (fourth row), the stress near the surface is somewhat smoother than after the previous events, but there is an even larger stress buildup at the fault bend. The chief observation that one can make, based on these three events, is that the effect of the free surface on fault stress may smooth itself out through time, but the effect of the fault bend builds up over time. The buildup of stress at the fault bend also furthers the argument that the stresses in the vicinity of the fault are much more complicated than what one would infer from resolving a constant tectonic stress field onto the upper and lower segments.

An interesting feature of all three sequential events is that the rupture front appears to have no difficulty breaking through the bend in the fault, even after the stress has started to build up there. Figure 11 compares rupture time contours for the first and second events. In the first event, the rupture front maintains elliptical symmetry, with faster rupture propagation in the mode II direction (up dip). The effect of the fault bend can be seen in the later rupture of the points at 10 km down dip. It appears that the rupture front initially skips the points at the bend, which are more difficult to rupture. Interestingly, the second rupture shows a very similar effect at the fault bend, even though the stresses there are much different from the first event. Here again, the rupture front jumps over the fault bend to the more easily ruptured points up dip. In this case, though, the decreased yield stress directly above the fault bend makes this process even easier and allows these points to rupture even more quickly. The rupture front contours near the free surface look very different between the two events, consistent with the very different stress distributions.

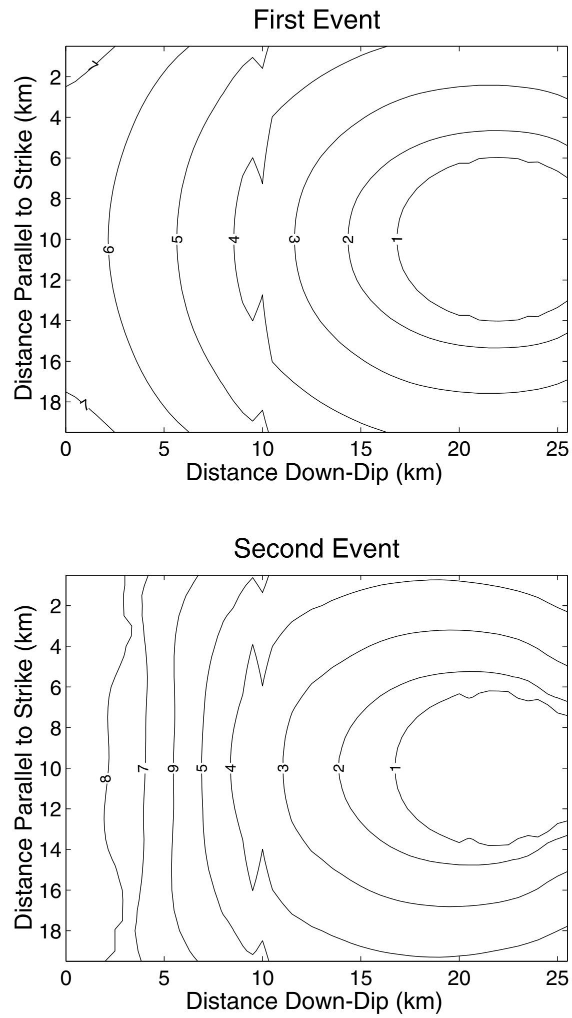

Figure 11. Comparison of rupture time contours for the first and second events. Contours are for 0 through 8 sec. Note that in both cases, the rupture front jumps across the fault bend (at 10 km down dip), but subsequently ruptures the entire fault.

The slip distributions resulting from the three events are shown in Figure 12. Each subfigure shows only the slip in the corresponding earthquake rather than the cumulative slip. Here we see that the second event, because it takes place on a fault with decreased stresses near the surface, has much less slip on the upper fault segment. The third event, however, because of the elevated shear prestress near its corners, has large slip near the surface. Interestingly, the slip distributions from the three events differ from each other more than do the slip distributions from the three different fault geometries shown in Figure 6. The peak ground velocities in Figure 13 show the differences between sequential earthquakes even more strikingly. The second and third events have much smaller peak ground motion, and the distributions are dissimilar in detail. The second event, because it had decreased stresses near the free surface, has much smaller ground motion than the first event, which had a high stress drop all the way to the surface. In addition, the motion dies out along strike because the upper corners of the fault did not rupture in this event. The third event, in contrast, has high ground velocity near the ends of the fault, where the high-stress regions nucleated rupture. There is also a secondary high point in peak velocity in the center of the fault along strike, where the two rupture fronts met. The effect of two rupture fronts colliding has also been seen in the planar dynamic fault models of Fukuyama and Madariaga (2000). Regardless of the differences in detail, there are still some unifying aspects of the peak ground velocity between the three sequential earthquakes: ground motion is strongly peaked at the fault trace, and there is much more motion on the hanging wall than on the footwall. Not shown in this figure, but also common among all the events, is a significant

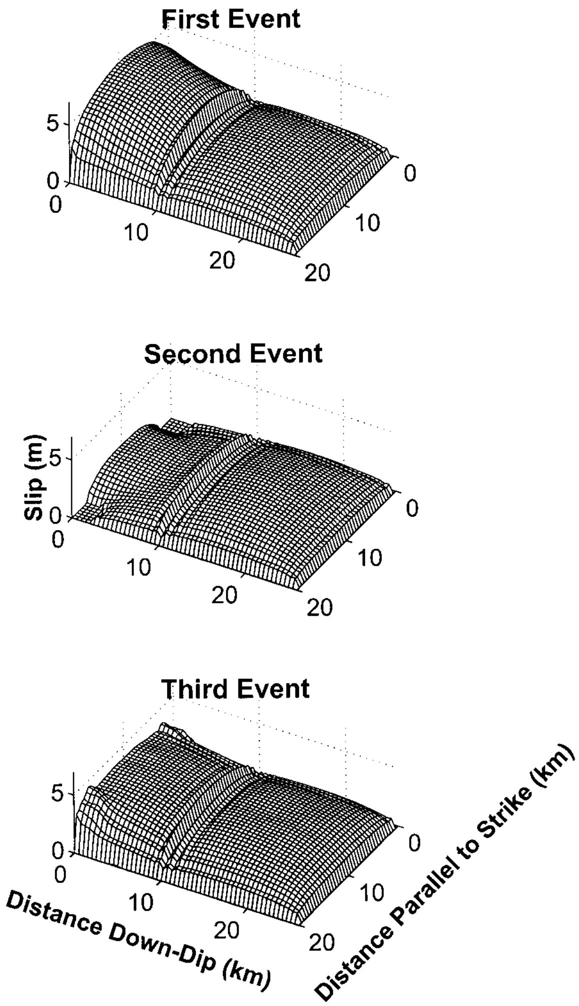

Figure 12. Slip distributions on the nonplanar fault from the first, second, and third earthquakes. The slip distributions are quantitatively different from each other. The greatest difference is near the free surface.

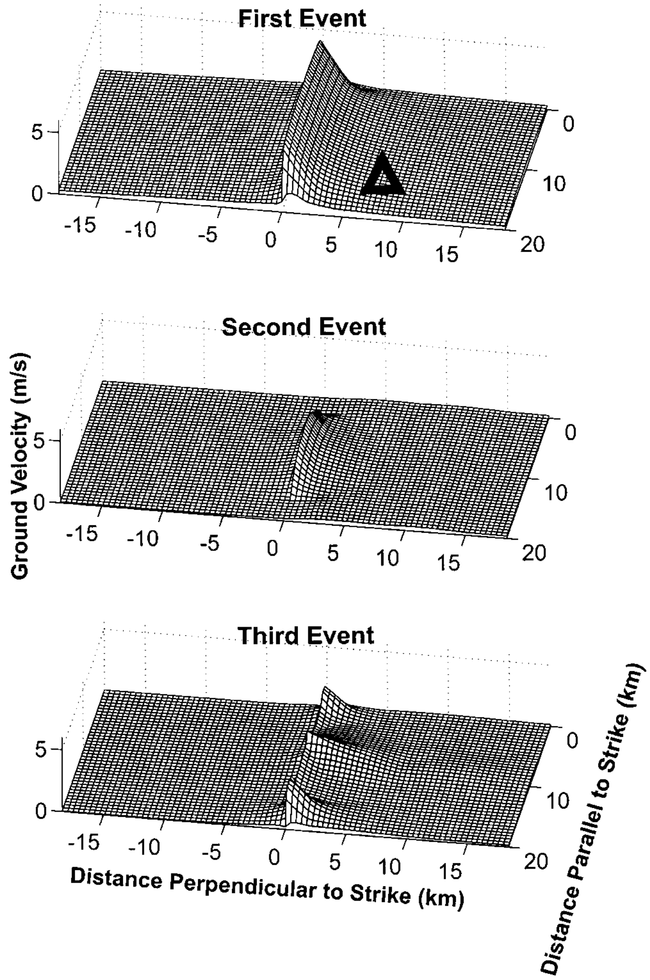

Figure 13. Peak ground velocity amplitude for the first, second, and third earthquakes on the nonplanar fault. All three ground velocity distributions are qualitatively different, but all display typical features associated with the dipping fault geometry. The location at which synthetic seismograms are later calculated is marked with a triangle on the top plot.

component of strike-slip motion on the upper edges of the faults. Thus, the general effects of the free surface on dipping faults are still seen, regardless of the complexity of the stress on the fault. It is important to note, however, that the details of ground motion are quite different between the three events, as seen in the synthetics (sampled at the point 15 km along strike and 3 km perpendicular to strike) in Figure 14. It is clear that the very different prestress patterns in the three events cause very different ground motion, even at low frequencies. It appears the effects of fault geometry are much more apparent in the overall spatial distribution of ground motion than in individual ground-motion records.

Discussion

The comparison between fault slip and ground motion for the nonplanar, 29°-dipping, and 53°-dipping faults indicates that the purely dynamic effects of a bend in a fault are not very large. This result is in agreement with the strike-slip faulting models of Aochi *et al.* (2000), Aochi and Fukuyama (2002), and Aochi *et al.* (2002), who found that the effect of a nonplanar fault on rupture propagation and slip was primarily due to different static shear prestress on the different fault segments. The current work shows that in the absence of this static effect, the ground motion from a nonplanar fault also does not show much of a signal from the fault bend. In addition, our initial comparison between a model with constant shear and normal stresses and two models with rotated shear and normal stresses indicates that for the deeply buried part of the fault, even the static stress field is not a large source of variability. This result is perhaps not very surprising: simple proximity would imply that the more deeply buried part of the fault would have less effect on the ground motion than the shallow segment. This proximity effect is further amplified by the large effect of the free sur-

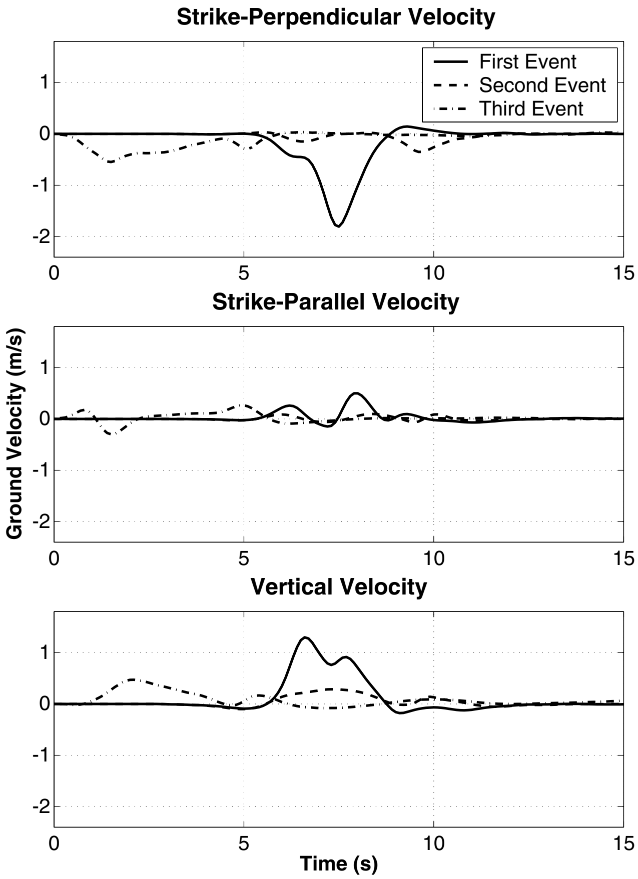

Figure 14. Synthetic ground velocity records for all three earthquakes on the nonplanar fault. Records are sampled at a point on the hanging wall approximately 15 km along strike and 3 km away from the fault trace (triangle on Fig. 13). This figure shows a comparison between the first event, the second event, and the third event. The records are qualitatively very different, reflecting the very different prestress pattern in each event.

face on the near-source ground motion. One might argue that the effect of the free surface is artificially amplified by the fact that in our models we have a roughly constant stress drop up to the free surface. However, models with the shear and normal stresses tapered down to zero on the upper fault segment show effects quite similar to what have been presented here. In such a case, the peak ground motion for the nonplanar fault is very similar to that of the 29°-dipping fault, although the area of high ground motion is somewhat broadened spatially.

The current study also explicitly includes the time variation of normal stress in the friction law. This could be an important factor, because the stress field radiated by rupture of one fault segment will in general induce changes in both normal and shear stress on the other segment. The effect of this process on friction could lead to the possibility of a larger dynamic (as opposed to static) effect of the fault bend than in Aochi *et al.* (2000). Aochi *et al.* (2002) argued that this effect is secondary compared to the dynamic changes in shear stress. While this may be true for the initial propagation of rupture onto another fault branch, the change in normal stress at the bend can reach very large levels over the course of an event and can have a noticeable effect on the final fault slip. Regardless, in our thrust faulting models, the effects of the fault bend are swamped by the effects of the angle between the shallow segment and the free surface. This result is in agreement with Oglesby and Day (2001a,b), who found that the spatial distribution of near-source peak ground motion in the 1999 Chi-Chi earthquake was dominated by the dipping fault geometry. It is possible, however, that a more deeply buried fault, which would not experience the free-surface effect, might display relatively more of an effect from buried structure. Additionally, when interpreting the results of this and all other fault dynamics studies, important attention should be given to the assumptions about the stress field. Our results imply that the effect of the fault bend may not be very important when the static stress field is not correlated with fault orientation. However, it is possible that models with different geometry (that can experience rupture with a single tectonic stress field) will give different results. The question of which type of model (or more likely, a model somewhere in between these extremes) is more appropriate for physical faults is certainly open and beyond the reach of this study.

The effect of the multiple earthquakes on our nonplanar fault is rather complicated due to different attributes of the fault geometry. Based on a small sample of three events, it is possible that the effects of the free surface on the fault stress near the surface (lowered thrust and normal stresses, induced strike-slip stresses) are converging to some sort of steady state. This behavior has been seen in the 2D thrust faulting models of Shi *et al.* (1998), who simulated many more events than the current study. The stress buildup at the fault bend, in contrast, appears to accumulate over multiple earthquakes. The final stress pattern after the third event is very complex, with strong variations in both components of shear stress, as well as a very large concentration in normal stress. The results here emphasize that when geometry is nontrivial, it is very important to consider variations in all stress components.

Another issue raised by the current results is the origin of complexity in stress, fault motion, and ground motion. For a planar fault, it is difficult to sustain strongly heterogeneous fault slip without a rate-weakening friction law (e.g., Nielsen and Olsen, 2000). The current models, which use a pure slip-weakening friction law, do indeed produce rather smooth slip distributions in the first three events. However, the fault stress becomes less uniform with every event, which could potentially lead to great complexity in slip in future events. In the current models, the fault bend does not serve as a barrier to rupture, but it is not clear if this behavior will continue over tens or hundreds of events: the stress buildup may eventually be too great for rupture to proceed across the fault segment boundary, confining rupture to the deeper or shallower segment. Alternatively, as suggested by Andrews (1989), a third fault segment may eventually grow from the fault bend, releasing the stress buildup. A larger-scale analog for our geometry may be found in the fault systems of eastern Taiwan, which likely are underlain by a shallow-dipping detachment (Carena *et al.*, 2002). This attachment steepens significantly down dip, and a zone of increased seismicity (possibly related to stress concentration) is found near this change in dip angle. A much larger catalog of events is required before any strong conclusions may be drawn about the long-term effects mentioned earlier. Regardless, the buildup of stress at the fault bend argues that to simply use a single tectonic stress field resolved onto the various fault branches (the rotated case) may not be very realistic in the branching area. Indeed, it is at these geometrical discontinuities that one would expect to see the widest divergence from such a homogeneous stress field.

The implications for multiple earthquake cycles must be viewed as somewhat tentative, however, because as noted, we have made no effort to model the interseismic stress buildup. In particular, it is likely that some sort of relaxation mechanism could smooth out the stress peaks, although it is unlikely to remove them completely. Therefore, a more cautious interpretation of these results might be simply to view the three events as three independent events with different, heterogeneous stress fields. Common features of all three events (such as amplified motion on the hanging wall and a kink in the slip distribution at the fault bend) may be thought of as robust features of the fault geometry, while other features (such as the overall amplitude and spatial pattern of the ground motion on the surface) are much more dependent on the details of the stress distribution. However, a systematic study of the effects of heterogeneous stress is beyond the scope of the current article.

A final issue is the question of what controls complexity in the slip and ground motion from earthquakes: fault geometry or stress distribution. The current results show that both are related. There is less of a difference between the slip and peak ground motion of the three different geometries than there is between the three sequential events on the bent fault. Taken by itself, this result would seem to imply that the different stress patterns of the three different ruptures are a more important factor than the fault geometry. However, even through the ground motions from the three sequential ruptures are different in detail, they share many common features, as noted earlier. Furthermore, the evolution of stress in this case is determined by the fault geometry, and the current results lead to the hope that such evolution could be predicted based on detailed knowledge of fault geometry.

Conclusions

The current models of a nonplanar thrust fault that intercepts the surface indicate that a change in dip at depth does not have a large effect on either the fault motion or the nearby ground motion if there is no systematic difference in the stress on the two fault segments. Both the fault and ground motion are dominated by the breakout phase that results when the fault rupture reaches the free surface. The behavior of the earthquake rupture near the free surface is in turn dominated by the dip angle between the shallow segment of the fault and the free surface. There are some limitations to this conclusion, however. This study concentrates on the purely dynamic effects of fault geometry and not on the associated static stress patterns possibly associated with a nonplanar fault. Also, we have only looked at the near-source ground motion, which is more likely to be dominated by the shallower portions of the fault. It is possible that at more distant observation points it may be possible to see more easily the separate signal from each fault segment. Finally, our simulations are numerically accurate only up to approximately 0.6 Hz, so our conclusions are also restricted to low frequencies. In spite of these caveats, the implication of the current results is that for the purposes of predicting near-source, low-frequency ground motion, knowledge of the deep structure of thrust faults may not be very important. This is especially true if the fault intersects the free surface, in which case the free-surface effect dominates the local ground motion. This result could have implications for seismic hazard near thrust faults such as those in the Los Angeles Basin, where the subsurface geometry is not very well constrained.

The main effect of the bend in our nonplanar fault is the buildup of a stress concentration at the change in dip over multiple earthquakes. Even though this stress buildup has little effect on the propagation of rupture and slip in the first three events, it could lead to greater complexity far into the future. However, the current study does not attempt to model the interseismic period other than as a process of linear stress scaling and does not include any form of aseismic stress relaxation or plastic flow, with the exception of a boxcar averaging of the stresses between events. If faults have a mechanism of releasing stress at geometrical discontinuities, stresses may eventually reach a steady state, and complexity may cease its growth. Additionally, nucleation is artificially imposed, rather than being a natural outgrowth of the interseismic loading. A simulation method that accurately models the interseismic stress loading, nucleation, and dynamic rupture is clearly needed to deal with such issues. Such a method will be the subject of future work.

Acknowledgments

This research was supported by LLNL/IGPP Grant 98-GS012 and by the National Science Foundation under Grant EAR-9725709. This article is ICS Contribution Number 0557. The authors gratefully acknowledge helpful conversations with Steve Day, Gary Axen, and Kim Olsen, as well as very useful reviews by Ruth Harris and an anonymous reviewer.

References

Andrews, D. J. (1976). Rupture velocity of plane strain shear cracks, *J. Geophys. Res.* **81,** 5679–5687.

Andrews, D. J. (1989). Mechanics of fault junctions, *J. Geophys. Res.* **94,** 9389–9397.

Andrews, D. J. (1999). Test of two methods for faulting in finite-difference calculations, *Bull. Seism. Soc. Am.* **89,** 931–937.

Andrews, D. J., and Y. Ben-Zion (1997). Wrinkle-like slip pulse on a fault between different materials, *J. Geophys. Res.* **102,** 553–571.

Aochi, H., and E. Fukuyama (2002). Three-dimensional nonplanar simulation of the 1992 Landers earthquake, *J. Geophys. Res.* **107,** doi 10.1029/2000JB000061.

Aochi, H., E. Fukuyama, and R. Madariaga (2002). Effect of normal stress during rupture propagation along nonplanar faults, *J. Geophys. Res.* **107,** doi 10.1029/2001JB000500.

Aochi, H., E. Fukuyama, and M. Matsu'ura (2000). Spontaneous rupture propagation on a non-planar fault in 3D elastic medium, *Pageoph* **157,** 2003–2027.

Axen, G. J. (1992). Pore pressure, stress increase, and fault weakening in low-angle normal faulting, *J. Geophys. Res.* **97,** 8979–8991.

Ben-Zion, Y., and D. J. Andrews (1998). Properties and implications of dynamic rupture along a material interface, *Bull. Seism. Soc. Am.* **88,** 1085–1094.

Bouchon, M., and D. Streiff (1997). Propagation of a shear crack on a nonplanar fault: a method of calculation, *Bull. Seism. Soc. Am.* **87,** 61–66.

Brune, J. (1996). Particle motions in a physical model of shallow angle thrust faulting. *Proc. Indian Acad. Sci. Earth Planet. Sci.* **105,** L197–L206.

Burridge, R. (1973). Admissible speeds for plane-strain self-similar shear cracks with friction but lacking cohesion, *Geophys. J. R. Astr. Soc.* **35,** 439–455.

Carena, S., J. Suppe, and H. Kao (2002). Active detachment of Taiwan illuminated by small earthquakes and its control of first-order topography, *Geology* **30,** 935–938.

Davis, P. M., and L. Knopoff (1991). The dipping antiplane crack, *Geophys. J. Int.* **106,** 581–585.

Day, S. M. (1982). Three-dimensional simulation of spontaneous rupture: the effect of nonuniform prestress, *Bull. Seism. Soc. Am.* **72,** 1881–1902.

Fukuyama, E., and R. Madariaga (2000). Dynamic propagation and interaction of a rupture front on a planar fault, *Pageoph* **157,** 1959–1979.

Hardebeck, J. L., and E. Hauksson (2001). Crustal stress field in southern California and its implications for fault mechanics, *J. Geophys. Res.* **106,** 21,859–21,882.

Harris, R. A., and S. M. Day (1993). Dynamics of fault interaction: parallel strike-slip faults, *J. Geophys. Res.* **98,** 4461–4472.

Harris, R. A., and S. M. Day (1997). Effects of a low-velocity zone on a dynamic rupture, *Bull. Seism. Soc. Am.* **87,** 1267–1280.

Harris, R. A., and S. M. Day (1999). Dynamic 3D simulations of earthquakes on en echelon faults, *Geophys. Res. Lett.* **26,** 2089–2092.

Harris, R. A., R. J. Archuleta, and S. M. Day (1991). Fault steps and the dynamic rupture process: 2D numerical simulations of a spontaneously propagating shear fracture, *Geophys. Res. Lett.* **18,** 893–896.

Harris, R. A., J. F. Dolan, R. D. Hartleb, and S. M. Day (2002). The 1999 Izmit, Turkey, earthquake; a 3D dynamic stress transfer model of intraearthquake triggering, *Bull. Seism. Soc. Am.* **92,** 245–255.

Heaton, T. H., and D. V. Helmberger (1979). Generalized ray models of the San Fernando earthquake, *Bull. Seism. Soc. Am.* **69,** 1311–1341.

Ida, Y. (1972). Cohesive force across the tip of a longitudinal shear crack and Griffth's specific surface energy, *J. Geophys. Res.* **77,** 3796–3805.

Kase, Y., and K. Kuge (1998). Numerical simulation of spontaneous rupture process on two non-coplanar faults: the effect of geometry on fault interaction, *Geophys. J. Int.* **135,** 911–922.

Lapusta, N., J. R. Rice, Y. Ben-Zion, and G. Zheng (2000). Elastodynamic analysis for slow tectonic loading with spontaneous rupture episodes on faults with rate- and state-dependent friction, *J. Geophys. Res.* **105,** 23,765–23,789.

Magistrale, H., and S. M. Day (1999). Three-dimensional simulations of multisegment thrust fault rupture, *Geophys. Res. Lett.* **26,** 2093–2096.

Mikumo, T., and T. Miyatake (1993). Dynamic rupture processes on a dipping fault, and estimates of stress drop and strength excess from the results of waveform inversion, *Geophys. J. Int.* **112,** 481–496.

Mount, V. S., and J. Suppe (1992). Present-day stress orientations adjacent to active strike-slip faults: California and Sumatra, *J. Geophys. Res.* **97,** 11,995–12,013.

Nielsen, S. B. (1998). Free surface effects on the propagation of dynamic rupture, *Geophys. Res. Lett.* **25,** 125–128.

Nielsen, S. B., and L. Knopoff (1998). The equivalent strength of geometrical barriers to earthquakes, *J. Geophys. Res.* **103,** 9953–9965.

Nielsen, S. B., and K. B. Olsen (2000). Constraints on stress and friction from dynamic rupture models of the 1994 Northridge, California, earthquake, *Pageoph* **157,** 2029–2046.

Oglesby, D. D. (1999). Earthquake dynamics on dip-slip faults, *Ph.D. Thesis*, University of California, Santa Barbara.

Oglesby, D. D., and S. M. Day (2001a). The effect of fault geometry on the 1999 Chi-Chi (Taiwan) earthquake, *Geophys. Res. Lett.* **28,** 1831–1834.

Oglesby, D. D., and S. M. Day (2001b). Fault geometry and the dynamics of the 1999 Chi-Chi (Taiwan) earthquake, *Bull. Seism. Soc. Am.* **91,** 1099–1111.

Oglesby, D. D., R. J. Archuleta, and S. B. Nielsen (1998). Earthquakes on dipping faults: the effects of broken symmetry, *Science* **280,** 1055–1059.

Oglesby, D. D., R. J. Archuleta, and S. B. Nielsen (2000a). The dynamics of dip-slip faults: explorations in two dimensions, *J. Geophys. Res.* **105,** 13,643–13,653.

Oglesby, D. D., R. J. Archuleta, and S. B. Nielsen (2000b). The three-dimensional dynamics of dipping faults, *Bull. Seism. Soc. Am.* **90,** 616–628.

Rudniki, J., and M. Wu (1995). Mechanics of dip-slip faulting in an elastic half-space, *J. Geophys. Res.* **100,** 22,173–22,186.

Scholz, C. H. (1990). *The Mechanics of Earthquakes and Faulting*, Cambridge U Press, New York.

Shi, B., A. Anooshehpoor, J. N. Brune, and Y. Zeng (1998). Dynamics of thrust faulting: 2D lattice model, *Bull. Seism. Soc. Am.* **88,** 1484–1494.

Sibson, R. H., and G. Xie (1998). Dip range for intracontinental reverse fault ruptures: truth not stranger than friction? *Bull. Seism. Soc. Am.* **88,** 1014–1022.

Whirley, R. G., and B. E. Engelmann (1993). DYNA3D: A Nonlinear, Explicit, Three-Dimensional Finite Element Code for Solid and Structural Mechanics—User Manual, UCRL-MA-1107254 Rev. 1, University of California, Lawrence Livermore National Laboratory.

Zoback, M. D., M. L. Zoback, V. S. Mount, J. Suppe, J. P. Eaton, J. H. Healy, D. H. Oppenheimer, P. A. Reasenberg, L. M. Jones, C. B. Raleigh, I. G. Wong, O. Scotti, and C. M. Wentworth (1987). New evidence on the state of stress of the San Andreas fault system, *Science* **238,** 1105–1111.

Department of Earth Sciences
University of California, Riverside
Riverside, California 92521
david.oglesby@ucr.edu
(D.D.O.)

Department of Geological Sciences
and Institute for Crustal Studies
University of California, Santa Barbara
Santa Barbara, California 93106
ralph@crustal.ucsb.edu
(R.J.A.)

Manuscript received 8 October 2002.